SCIENTIFIC REPORTS

OPEN

SUBJECT AREAS:
DNA METABOLISM
CHROMOSOMES

Received
28 April 2014

Accepted
11 June 2014

Published
26 June 2014

Correspondence and requests for materials should be addressed to S.L. (Shunwen.Lu@ars.usda.gov)

Zn^{2+} Blocks Annealing of Complementary Single-Stranded DNA in a Sequence-Selective Manner

Shunwen Lu

USDA-ARS, Cereal Crops Research Unit, Fargo, ND 58102, USA.

Zinc is the second most abundant trace element essential for all living organisms. In human body, 30–40% of the total zinc ion (Zn^{2+}) is localized in the nucleus. Intranuclear free Zn^{2+} sparks caused by reactive oxygen species have been observed in eukaryotic cells, but question if these free Zn^{2+} outrages could have affected annealing of complementary single-stranded (ss) DNA, a crucial step in DNA synthesis, repair and recombination, has never been raised. Here the author reports that Zn^{2+} blocks annealing of complementary ssDNA in a sequence-selective manner under near-physiological conditions as demonstrated *in vitro* using a low-temperature EDTA-free agarose gel electrophoresis (LTEAGE) procedure. Specifically, it is shown that Zn^{2+} does not block annealing of repetitive DNA sequences lacking CG/GC sites that are the major components of junk DNA. It is also demonstrated that Zn^{2+} blocks end-joining of double-stranded (ds) DNA fragments with 3′ overhangs mimicking double-strand breaks, and prevents renaturation of long stretches (>1 kb) of denatured dsDNA, in which Zn^{2+}-tolerant intronic DNA provides annealing protection on otherwise Zn^{2+}-sensitive coding DNA. These findings raise a challenging hypothesis that Zn^{2+}-ssDNA interaction might be among natural forces driving eukaryotic genomes to maintain the Zn^{2+}-tolerant repetitive DNA for adapting to the Zn^{2+}-rich nucleus.

Zinc is the second most abundant trace element (after iron) essential for all living organisms[1]. Within the cells, zinc exists as a redox-stable divalent cation (Zn^{2+}) which primarily coordinates with proteins as structural components or catalytic cofactors[2]. The total number of Zn^{2+}-binding proteins has been reported to be 2,800 and 2,042, respectively in the human[3] and Arabidopsis[4] genomes. It is known that dietary zinc ions are taken up rapidly by the nucleus[5] of the mammalian cells that accumulate more than one third (30–40%) of the intracellular zinc ions[1]. This nucleus-predominant distribution reflects the fact that many DNA synthesis/transcription-related proteins are Zn^{2+}-dependent, e.g., DNA polymerase alpha-primase[6] and RNA polymerase II[7], each contains six and eight zinc atoms per molecule, respectively. Intranuclear free Zn^{2+} sparks caused by reactive oxygen species have been observed in mammalian cells under oxidative stress[8,9], but if these Zn^{2+} outrages could affect annealing of complementary single-stranded (ss) DNA, a crucial step in DNA synthesis, repair and recombination[10] is yet unknown.

Previous studies on Zn^{2+}-DNA interactions were mainly focused on double-stranded (ds) DNA. It has been shown that Zn^{2+} promotes renaturation of denatured dsDNA, destabilizes or stabilizes the double helix of specific DNA sequences[11,12], causes DNA bending[13] and kinking[14], and induces transition from the right-handed B-DNA to other unusual forms such as the left-handed Z-DNA[15], Z-DNA-related *Z DNA[16], triple-stranded *H-DNA[17], and metal-DNA complexes so-called M-DNA[18]. The biological relevance of the Zn^{2+}-induced conformational perturbations on dsDNA has not been well established, largely due to that the related studies often involve non-physiological conditions.

In this work, a simple low-temperature EDTA-free agarose gel electrophoresis procedure (LTEAGE) was developed and used to characterize the Zn^{2+}-ssDNA interaction coupling with UV-Vis spectrum and fluorescence quenching analyses. The presented data indicate that Zn^{2+} interacts with ssDNA and blocks the annealing of complementary strands in a sequence-selective manner under near-physiological conditions, and such blocking effects may impact DNA replication/repair-associated processes such as the end-joining of DNA double-strand breaks and the annealing of long stretches of ssDNA involved in homologous recombination. It also suggests that the repetitive junk DNA widely spread among eukaryotic genomes might provide annealing protection on the otherwise Zn^{2+}-sensitive coding-DNA. The biological relevance of these findings is discussed

while examining the distribution of Zn^{2+}-tolerant junk DNA in representative chromosomes of humans and plants such as wheat.

Results

Zn^{2+} blocks annealing of complementary ssDNA with a preference for G+C-"rich" sequences. For initial tests, four sets of complementary short DNA oligos (25–33 nt) were synthesized based on the wheat actin gene (*ACT1*). ACT1-E25 (25 nt, G+C 60%) and ACT1-E26 (26 nt, G+C 50%) were designed to the second and third exon, respectively, and ACT1-I26 (26 nt, G+C 42.3%) and ACT1-I33 (33 nt, G+C 30.3%) to the second intron of the *ACT1* gene (Supplementary Table S1). LTEAGE tests (Fig. 1a) revealed that the annealing of the relatively G+C-"rich" ACT1-E25 or ACT1-E26 oligos was apparently reduced when the complementary ssDNA was pre-treated with 100 μm Zn^{2+} and completely blocked when the Zn^{2+} concentration increased to 250 μm, as indicated by the absence of dsDNA-specific bands, and in contrast, the annealing of the A+T-rich ACT1-I26 or ACT1-I33 was only reduced by Zn^{2+} at ≥250 μm, as indicated by the gradually weakened dsDNA bands (Fig. 1b). The blocking effects were abolished when EDTA, which is a strong chelator of divalent metal ions[19], was added to the annealing solutions (lanes 9), indicating that the blocking was indeed caused by Zn^{2+}. Variations in salt concentrations within the ranges determined for the nucleus of eukaryotic cells (e.g., 10–30 mM NaCl)[20,21] did not change the annealing patterns significantly under the same Zn^{2+} treatments (data not shown). Three other divalent metal ions including Mg^{2+} and Mn^{2+} (Supplementary Fig. S1) as well as Ca^{2+} (data not shown) did not affect the annealing under the same conditions, or even at higher (up to 2 mM) concentrations. Incubation of pre-annealed dsDNA with Zn^{2+} did not cause disassociation of the double helix (Supplementary Fig. S2). These results indicated that the blocking of the annealing process was due to Zn^{2+}-ssDNA interaction.

UV-Vis spectrum analysis was done to detect Zn^{2+}-induced conformational perturbations in ssDNA solutions. It was found that Zn^{2+} caused a significant increase in the A295/A260 ratio of all four tested ssDNA samples when added at concentration ≥ 500 μm with the maximum found at 750 μm (Fig. 1c). However, the minimal concentration causing an increase in the A295/A260 ratio differed: it was found at 100 μm for both the plus (+) and minus (-) strands of ACT1-E25, and for the plus strand of ACT1-E26 in contrast to 250–500 μm for the complementary strands of ACT1-I26 and ACT1-I33 (Fig. 1c, arrows). The observed A295/A260 ratio changes in the tested concentrations (e.g., 10–750 μm Zn^{2+}) were not due to DNA precipitation as confirmed in separate experiments (data not shown); this was in consistence with a previous report that Zn^{2+} causes DNA precipitation with minimal concentrations at millimolar ranges, e.g., >1 mM[22].

To enable a comparative analysis, the A295/A260 ratios (A*) were further normalized using the formula $(A^*_{250}- A^*_0)/A^*_0$, in which A^*_{250} and A^*_0 stands for the A295/260 ratio for the sample containing metal ions at 250 μm and the blank control, respectively. For convenience, the calculated value was represented by the symbol "SD^Z" to indicate "Single-stranded DNA Zn^{2+}-binding potential". This method was adapted solely for the comparative analysis of the UV-Vis spectrum data, not attempted to substitute for dissociation constant (K_d) (which cannot be determined in this study due to technical restraints). The calculated SD^Z for the +/− strands of ACT1-E25 (G+C 60%), ACT1-E26 (G+C 50%), ACT1-I26 (G+C 42.3%) and ACT1-I33 (G+C 30.3%) was 1.14/1.22, 1.00/0.75, 0.89/0.86 and 0.50/0.16, respectively (Fig. 1c, Supplementary Table S2). Neither Mg^{2+} nor Mn^{2}+ caused significant changes in the A* values under the same conditions (Fig. 1c) or affected the annealing process of any ssDNA samples in the LTEAGE tests shown in Supplementary Fig. S1. These results confirmed that Zn^{2+} binds to ssDNA and the binding potential is likely determined by the G+C content of the targeted ssDNA molecules.

Fluorescence quenching assays were done to verify that the Zn^{2+} blocking event occurred independent of agarose gel electrophoresis conditions. Relative fluorescence units (RFU) were monitored in solutions containing the dual-labelled ACT1-E25 probe and its complementary strand pre-treated with metal ions (Fig. 1d). As shown in Fig.1e, the RFU started to decrease significantly when Zn^{2+} was added at a concentration as low as 50 μM, and reached the lowest levels (5–10%) at 250-500 μM. Neither Mg^{2+} nor Mn^{2+} caused a RFU reduction; instead, Mg^{2+} appeared to enhance annealing efficiency at ≥250 μM. These data confirmed that Zn^{2+} was able to block the annealing of sensitive ssDNA like ACT1-E25 at an even lower concentration (50 μM).

Zn^{2+} does not affect annealing of simple repetitive DNA sequences lacking CG/GC sites. To determine how the individual nucleotides contribute to the Zn^{2+} binding potential of a given ssDNA, oligos composed of different simple repeats were synthesized (Supplementary Table S1) and subjected to LTEAGE and UV-Vis spectrum analyses. It was found that the annealing between all types of complementary simple repeats that lack CG/GC sites were not or only slightly affected when Zn^{2+} was added at a concentration up to 750 μm. These Zn^{2+}-"tolerant" repetitive DNA included the mononucleotide repeats poly(dA)/(dT) and poly(dG)/(dC) (Fig. 2a), the dinucleotide repeats poly(dT-dG)/(dC-dA) and poly(dT-dC)/(dG-dA) (Fig. 2b), the trinucleotide repeats-like sequences such that associated with the wheat gypsy-type retrotransposon[23] and the hexanucleotide repeats such as the TTAGGG motifs found in the telomeric ends of all human chromosomes[24] (Fig. 2c). The other two types of dinucleotide repeats, i.e., poly(dC-dG)/(dG-dC) and poly(dA-dT)/(dT-dA) cannot be tested *per se* because of the self-complementarity. To demonstrate the vulnerability of the CG/GC sites to Zn^{2+} blocking, two sets of DNA oligos consisting of non-self complementary CG or TA repeats were designed: dCG-24 which contains six CG repeats separated by continuous G bases, and dTA-24 which has two TA repeats flanked by continuous T or A bases (Supplementary Table S1). The annealing of dTA-24 was reduced but never completely blocked, and in contrast, the annealing of dCG-24 was apparently reduced at 100 μm and almost completely blocked at ≥250 μm (Fig. 2d).

UV-Vis spectrum data indicated that the A* values of poly(dA) remained unchanged at all Zn^{2+} concentrations and those of other three mononucleotide repeats increased significantly only at higher concentrations (≥250 μm), and the calculated SD^Z was all relatively low (≤1.0) (Fig. 2e, Supplementary Table S2). Similarly, the A* values were also found to increase significantly only at higher concentrations (≥250 μm) for all dinucleotide repeats except for poly(dT-dG) and dGC-24, both of which were found at 100 μm, and the SD^Z was all low (≤1.0) except for poly(dT-dC) having SD^Z = 2.1 (Fig. 2f, Supplementary Table S2); These data suggested that the "tolerance" to Zn^{2+} blocking was due to the low Zn^{2+}-binding potential (e.g., SD^Z <1) associated with one or both complementary strands of the simple repetitive DNA, e.g., dTA-24/dAT-24 (SD^Z= 0.0 *vs*. 0.13) and poly(dT-dC)/(dG-dA) (SD^Z = 2.1 *vs*. 0.5) (Supplementary Table S2). This was also true for the *ACT1*-derived random sequences, e.g., the Zn^{2+}-tolerant ACT1-I26 and I-33 oligos had a low (0.17–0.89) SD^Z for both strands (Fig. 1c). But this rule does not apply for the dCG-24 oligos, which had lower SD^Z values for both strands (0.42 and 0.73, respectively) but annealed poorly (Fig. 2d, bottom). For the plus strand, this was likely due to the potential to form a G-quartet-like structure characteristic of repeated three-guanines separated by 3 to 5 T, A or G residues as described in previous studies[25]. The ssDNA with this unusual secondary structure had a high A295/260 ratio as shown in the blank control (0.19 *vs* 0.02–0.12

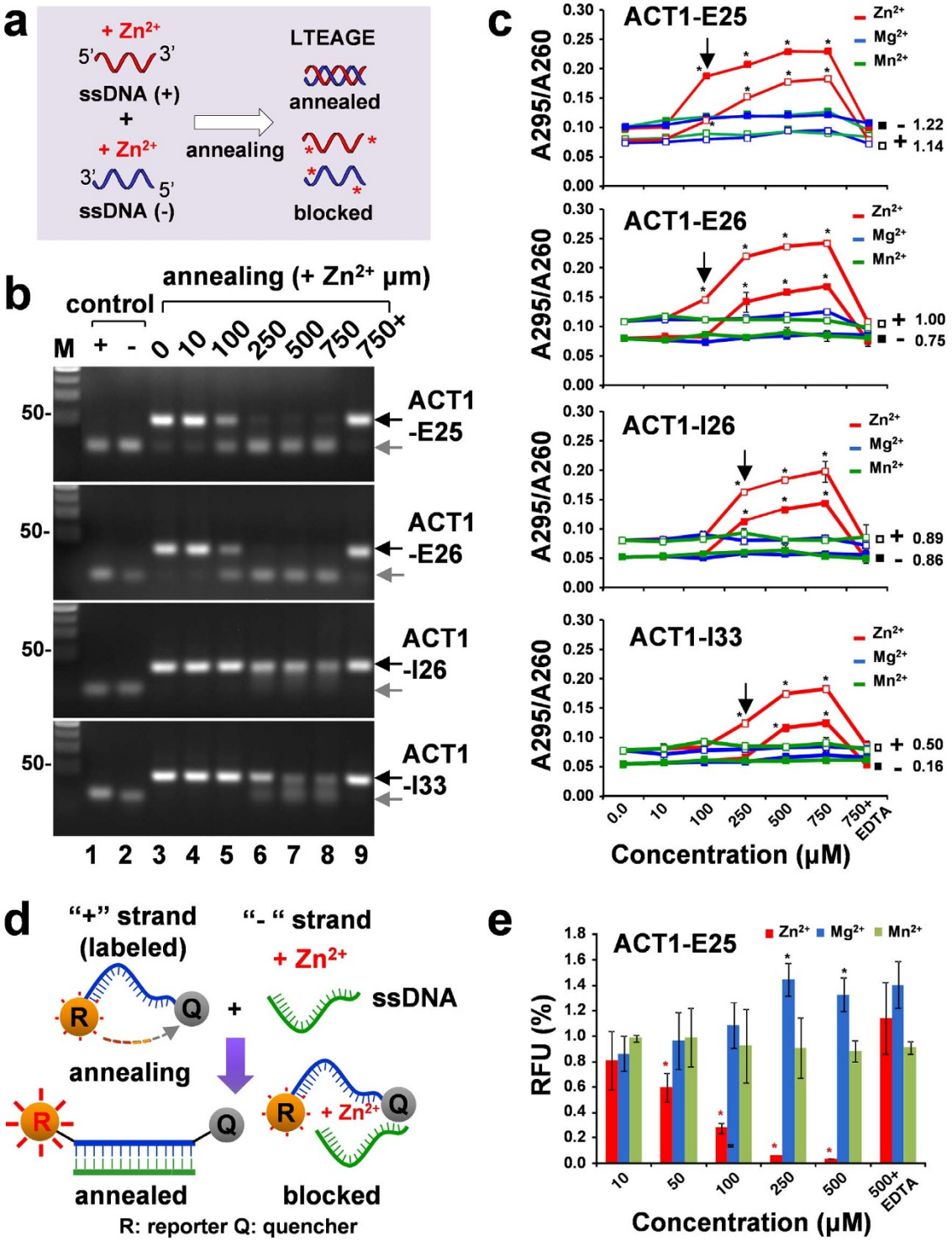

Figure 1 | Zn^{2+} blocks annealing of complementary ssDNA in a sequence-selective manner. (a) LTEAGE procedure. (b) Ethidium bromide (EtBr)-stained 2.5% agarose gels showing the annealing patterns. Control lanes were loaded with ssDNA (+ or – strand) without Zn^{2+} treatment. Lanes 9 were loaded with EDTA-treated (1 mM) samples. Double/single-stranded DNA-specific bands are indicated by black and gray arrows, respectively. M: 50-bp DNA ladder; (c) A295/A260 ratios plotted against metal ion concentrations. Arrows indicate the first points at which the ratio increased significantly. Numbers on the right of the strand symbols indicate the corresponding SD^Z values (at 250 μm). (d) and (e) Fluorescence quenching assay. Bars in (c) and (e) indicate standard deviations, most of which in (c) are masked by the squares representing the means; asterisks indicate significant differences (*t*-test, $P<0.05$).

for most oligos), leading to a lower SD^Z [calculated using the formula $(A^*_{250}- A^*_0)/A^*_0$ as mentioned above]. Thus, the SD^Z values of the dCG-24-like ssDNA with G-quartet-like structures are not comparable with other CG/GC-sites-containing random sequences with respective to the annealing events. Different methods are needed to resolve this issue. However, the C base-lacking telomere end-specific oligo (Supplementary Table S1), which is also expected to form G-quartet-like structures, was found to be Zn^{2+}-tolerant (Fig. 2c). This suggested that CG/GC sites (which are present in dCG-24 but not in the telomere end-specific oligo) are important for the observed Zn^{2+}

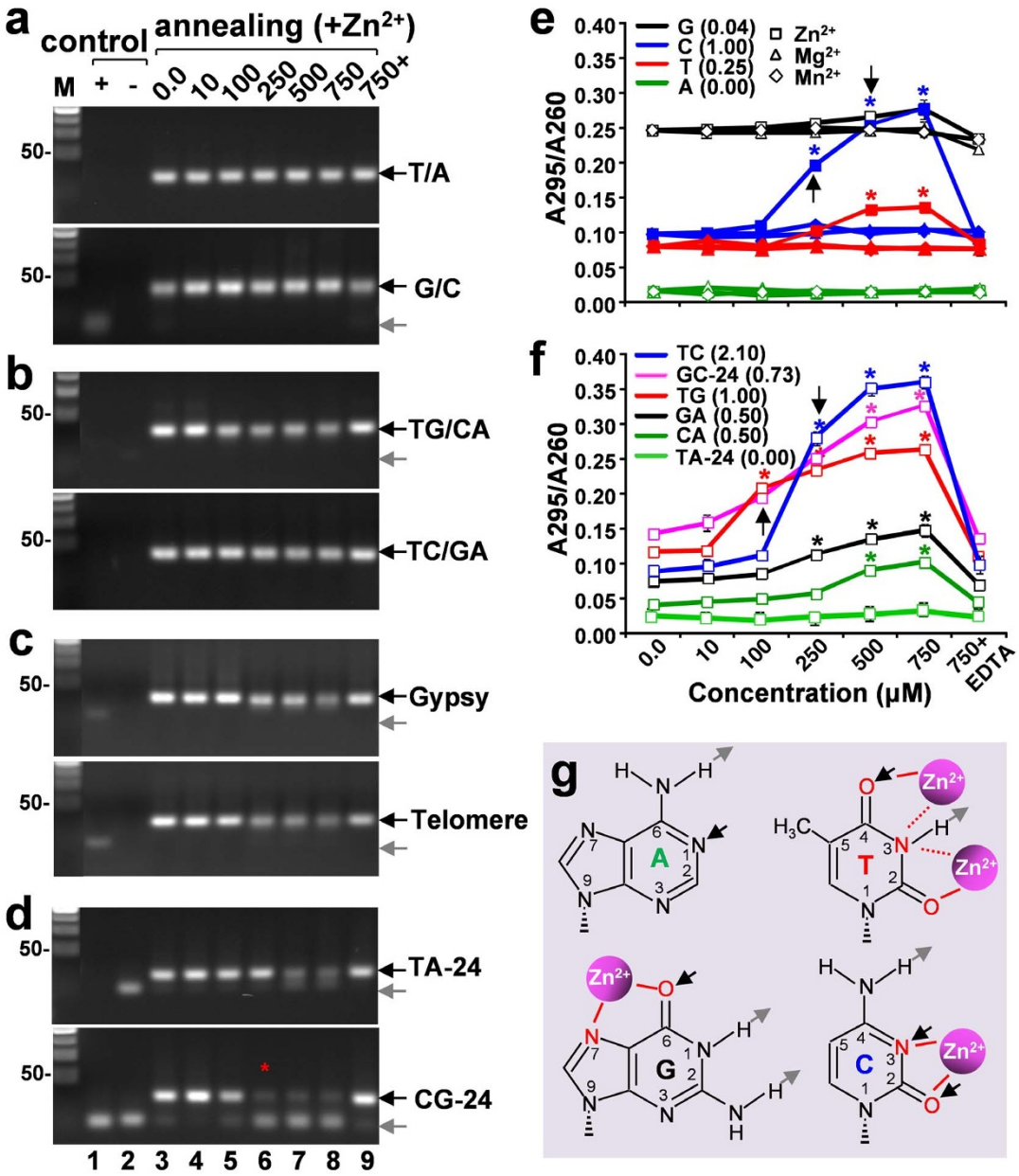

Figure 2 | Annealing patterns and Zn^{2+} binding potentials of ssDNA composed of repetitive nucleotides. (a–d). EtBr-stained 2.5% agarose gels showing the annealing patterns of mononucleotide (a), dinucleotide (b), tri- or hexanucleoride repeats (c), and the ssDNA containing CG or TA-repeats (d). Note that although the equal amounts of DNA were loaded, some ssDNA controls (e.g., lanes 1 and 2 in a–c) were not (or only faintly) visible because these CG/GC sites-lacking DNA oligos are not expected to form stable helical structures (as those shown in Fig. 3) that are preferentially targeted by EtBr, a well-known double helical DNA intercalator. (e and f). A295/A260 ratios plotted against metal ion concentrations as shown in Fig. 1. (g) Potential Zn^{2+} binding sites in the four types of nucleotides. The O and N atoms in the heterocyclic rings are highlighted in red. Hydrogen-bonding donors and receptors are indicated by gray and black arrows, respectively (adapted from ref. 10). Pink spheres representing the coordinated Zn^{2+}-water complex (ref. 26). Note that adenine lacks O atom and the N3 atom of thymine may not be a preferred binding site for Zn^{2+} (dashed lines) due to its bonding with the proton.

blocking effects. This was further tested by site-specific mutational analysis (see below).

The Zn^{2+}-binding potential of ssDNA was found to correlate with the chemical structures of compositional nucleotides. Adenine is the only one lacking an oxygen (O) atom; thymine is the only one lacking a deprotonated nitrogen (N) atom in the heterocyclic rings whereas guanine and cytosine have both O and one or more deprotonated N atoms (Fig. 2g). Previous studies have shown that divalent metal ions like Mg^{2+} and Zn^{2+} prefer to bind to G, C and T bases in a bidentate manner, i.e., bonded through an oxygen (O) and a nitrogen (N) atoms simultaneously[26]. Thus, poly(dA) and poly(dT-dA) would have the lowest SD^Z because of the lack of bidentate sites; poly(dC) and poly(dT-dC) would have the highest SD^Z because cytosine has a bidentate site which is always accessible due to the lack of intramolecular base paring, but ssDNA consisting of only CG/GC repeats like the minus strand of the dCG-24 oligos (Supplementary Table S2) would have a low SD^Z because the frequent intramolecular C-G base paring would inactivate some bidentate sites (Fig. 2e–2g). On the other hand, in a random sequence consisting of all four types of nucleotides, the bidentate sites on G/C bases could remain open depending on the potential of C-G base pairing that is determined by the nucleotide sequences of a given ssDNA. Thus, for most random sequences, the higher the G+C content, the higher the Zn^{2+} binding potential (e.g., $SD^Z > 1$) as shown for the *ACT1*-derived sequences (Fig. 1c, Supplementary Table S2).

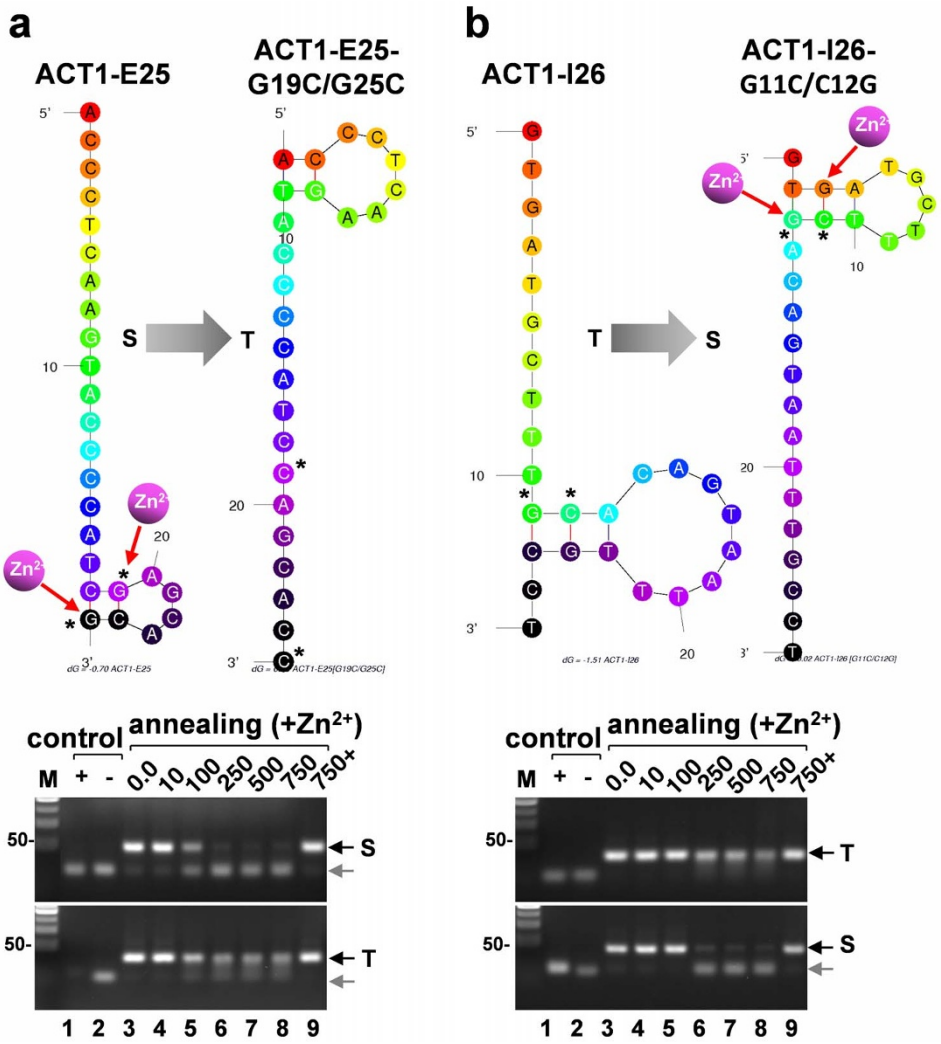

Figure 3 | DNA folding and site-specific mutational analyses reveal the hairpin structures potentially targeted by Zn^{2+} that prevent ssDNA annealing. (a). Point mutations that eliminate the CG/GC helix in the Zn^{2+}-sensitive (S) ACT1-E25 leads to a Zn^{2+}-tolerant (T) mutant (ACT1-G19C/G25C). (b) Point mutations that introduce a TG/GC helix in the Zn^{2+}-tolerant ACT1-I26 results in a Zn^{2+}-sensitive mutant (ACT1-I26-G11C/C12G). One representative folding structure predicted to be stable (with smaller ΔG) was chosen for each ssDNA as shown at the top. Colors in circles indicate the probability (0.001/black - 0.999/red) for the coded bases to be single stranded upon folding of the ssDNA. Mutation sites are indicated by asterisks. The guanine bases potentially targeted by Zn^{2+} are indicated by red arrows. Hydrogen bonds between C and G bases are highlighted in red. EtBr-stained 2.5% agarose gels showing the annealing patterns are given below (see Figure 1b for related legends).

Zn^{2+} blocks ssDNA annealing likely by targeting the CG/GC-like helix in the hairpin stem. Site-specific mutational analysis was performed to explore the structural basis of the Zn^{2+}-specific blocking event. DNA folding analysis revealed that all Zn^{2+}-"sensitive" ssDNA sequences are likely to form hairpins with a helical stem consisting of CG/GC or TG/GC external closing pairs. For example, in ACT1-E25, the last two bases (-CG_{25}) at the 3′ end would fold back to form a hairpin-like structure resulting in a 2-bp helix with C_{18}-G_{25} as the 5′ external closing pair (Fig. 3a). In ACT1-E26, the last three bases (-CCG_{26}) would fold back giving rise to a 3-bp helix (TGG/GCC) with T_{11}-G_{26} as the 5′ external closing pair through wobble paring[10] (Supplementary Fig. S3a). Both ACT1-I26 and ACT1-I33 would form hairpin-like structures but the resulted helices all lack CG/GC-like base pairs at the 5′ end of the helical stem. ACT1-I26 would have a 3-bp helix (GGA/CCT) with G_{11}-C_{24} as the 5′ external closing pair (Fig. 3b) and ACT1-I33 would have a 5-bp helix (ACTGC/GCATT) with A_{17}-T_{32} as the 5′ external closing pair (Supplementary Fig. S3b). Site-specific mutations depriving the CG/GC-like helices in ACT1-E25 conferred Zn^{2+} "tolerance" (i.e., the annealing *was not* blocked) as shown for the ACT1-E25-G19C/G25C mutant (Fig. 3a) whereas the mutations introducing new hairpin stems with a 5′ end CG/GC-like helix led to Zn^{2+} "sensitivity" (i.e., the annealing *was* blocked) as shown for the ACT1-I26- G11C/C12G mutant (Fig. 3b) and also for the ACT1-I33-G20C/C21G mutant (Supplementary Fig. S3b). Mutations made to the TG/GC helix of ACT1-E26 did not change the Zn^{2+} sensitivity because the ACT1-E26-C7G/G26C mutant gained a new helical stem with 5′ GG/CC external closing pairs (Supplementary Fig. S3a). In addition, sequential mutations were made to the Zn^{2+}-tolerant poly(dT-dG) which became Zn^{2+}-sensitive only when the mutations had led to a hairpin stem with TG/GC as the 5′ external closing pairs (Supplementary Fig. S4). These results confirmed that the CG/GC (TG/GC or GG/CC) helices derived from the 5′ external closing pairs in the hairpin stems of ssDNA were likely targeted by Zn^{2+} in the blocking events. This model was consistent with a previous X-ray structure study which suggested that Zn^{2+} binds to G bases in the 5′ end external closing pairs of a hairpin DNA by coordinating with the N7 atom and an O atom of a phosphate group associated with the adjacent nucleotide[27].

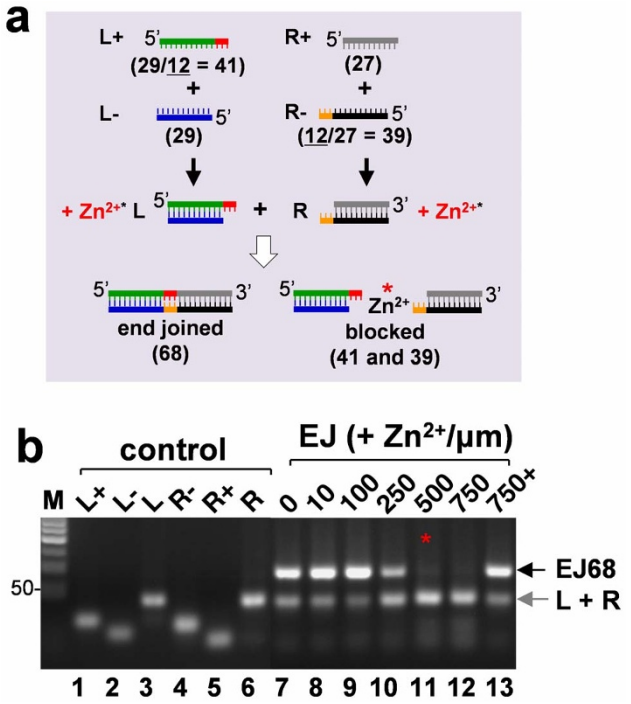

Figure 4 | Zn^{2+} blocks the end joining (EJ) of double-stranded DNA fragments mimicking double strand breaks (DSBs). (a) Procedures to generate DSBs. Oligos (L+/− and R+/−) are drawn in different colors with the 3′ overhangs highlighted in red or orange. Numbers (in nt/bp) indicate the size of DNA. (b) EtBr-stained agarose gels showing the end-joining patterns. Red asterisks indicate the point at which EJ was completely blocked. Note that the EJ event was not complete as seen in the control (lane 7), probably due to the lack of a DNA ligase (not included) for filling the gap at the EJ points. Control lanes were loaded with ssDNA (L+/− or R+/−) or DSB (L or R) alone without Zn^{2+} treatment. Lane 13 was loaded with EDTA-treated (1 mM) samples containing the two DSBs. End-joined and blocked DSBs-specific bands are indicated by black and gray arrows, respectively. M: 50-bp DNA ladder.

Zn^{2+} blocks the end joining of dsDNA fragments with short 3′ overhangs. The DNA oligo-based annealing assay mentioned above provided a simple way to evaluate the Zn^{2+}-specific blocking effects on the annealing process, but it is not suitable for testing even shorter (e.g., <15 bp) sequences that cannot be resolved clearly on agarose gels. To overcome this drawback, a pair of dsDNA fragments was designed, in which each dsDNA fragment carried a 12-nt complementary 3′ overhang containing Zn^{2+}-sensitive CG site (Supplementary Table S1), so that the annealing outcome can be easily monitored based on the success or failure of the end joining (EJ) between the two compatible dsDNA fragments in response to the Zn^{2+} treatment (Fig. 4a).

LTEAGE tests revealed that the EJ event was apparently reduced by Zn^{2+} at 250 μm and completely blocked at ≥500 μm (Fig. 4b). The 68-bp dsDNA product of the EJ event was well separated from the two dsDNA fragments (27 and 29 bp, respectively, excluding the 3′ overhang), and also distinguishable from the ssDNA samples consisting of the two complementary strands (27 to 41 nt) of the respective dsDNA fragment. The dsDNA fragment-specific bands but not the ssDNA-specific bands were clearly seen on the gel lanes loaded with the Zn^{2+}-blocked samples (lanes 11 and 12), indicating that the absence of the EJ event was due to the failure of the annealing between the two complementary 3′ overhangs carried by the two dsDNA fragments, not the results of any Zn^{2+}-induced disassociation of the double helix of each dsDNA molecule. Neither Mg^{2+} nor Mn^{2+} affected the EJ events under the same conditions

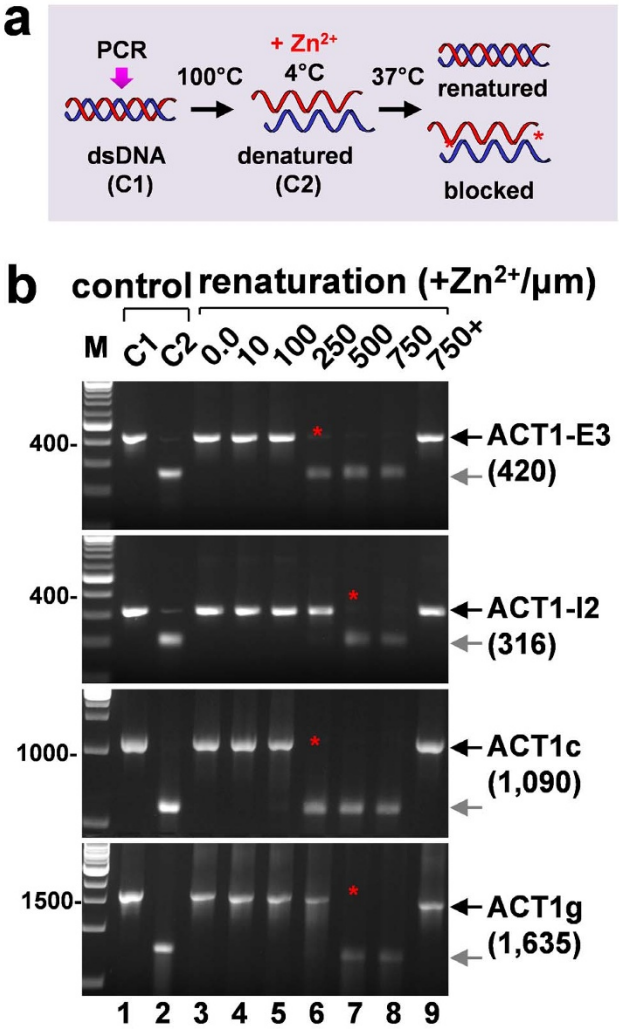

Figure 5 | Zn^{2+} blocks the renaturation of denatured dsDNA. (a) Experimental procedures. C1, control 1 (intact dsDNA); C2, control 2, denatured DNA (kept on ice to preserve the single-stranded status). (b) EtBr-stained 1.0% agarose gels showing the renaturation patterns of the denatured DNA fragments indicated on the right (numbers in parentheses indicate the size, in bp). Red asterisks indicate the points at which annealing was completely blocked. Gels are labeled in a similar way as shown in Figure 1b. M, 100 bp (top two panels) or 1 kb (bottom two panels) DNA ladders. Numbers on the left indicate the positions of size markers.

(Supplementary Fig. S5). These results confirmed that Zn^{2+} was able to block the annealing between complementary ssDNA as short as 12 nt, which is within the size range of ssDNA intermediates involved in the double-strand breaks (DSBs)-associated DNA repair processes such as the microhomology-mediated end joining pathway[28].

Zn^{2+} blocks the renaturation of denatured dsDNA with a preference for coding sequences. To test the Zn^{2+} blocking effects on the annealing of even longer ssDNA without oligo synthesis limitations, DNA denture-renaturation tests were performed using dsDNA amplified by PCR as illustrated in Fig. 5a. Four dsDNA fragments (316–1,635 bp) were amplified from the wheat *ACT1* gene. Two of them were amplified from the coding sequences with ACT1-E3 (420 bp, G+C 52.3%) from the third exon only, and ACT1c (1,090 bp, G+C 52.9%) from the coding region involving three exons. The other two were amplified from genomic DNA with ACT1-I2 (316 bp, G+C 33.8%) from the second intron only, and

ACT1g (1,635 bp, G+C 44.7%) from the entire open reading frame (Supplementary Table S3).

LTEAGE tests revealed that the renaturation of the exonic ACT1-E3 (420 bp) was completely blocked by Zn^{2+} at 250 μm whereas that of the intronic ACT1-I2 (316 bp) was blocked by Zn^{2+} at 500 μm, twice higher than that of ACT1-E3 (Fig. 5b, lanes 6 and 7, top two panels).The renaturation of the coding DNA-derived 1,090-bp ACT1c, which was more than twice longer than ACT1-E3, was also completely blocked by Zn^{2+} at 250 μm (third panel). In contrast, the 1,635-bp ACT1g fragments, which contained three A+T-rich introns, renatured perfectly at the same concentration (bottom panel).These results indicated that minimal Zn^{2+} concentrations blocking the annealing of short (24–26 nt) DNA oligos (e.g., Fig. 1b and 2d) were sufficient to prevent the annealing of G+C-rich coding DNA with the size >10 times longer (420–1,090 bp), and more importantly, the Zn^{2+}-tolerant intronic sequences provided annealing protection on the Zn^{2+}-sensitive coding DNA when the two join together as compared with ACT1c and ACT1g (lanes 6 and 7, red asterisks). Interestingly, unlike the ACT1-I26 and ACT1-I33 DNA oligos, both of which were tolerant to Zn^{2+} blocking up to 750 μm (Fig. 1b), the 316-bp ACT1-I2 fragment which contained both ACT1-I26 and ACT1-I33 sequences from the same intron region became Zn^{2+}-sensitive at 500 μm (Fig. 5b, the second panel from top). This was likely due to that the ACT1-I2 fragment actually contained short (13 and 10 bp, respectively) flanking exonic sequences incorporated into the PCR primers due to technical requirements (Supplementary Table S3) that would give rise a hairpin stem containing a GG/CC helix at the 5′ end as predicted by DNA folding analysis (data not shown); this *de novo* hairpin structure could have partially offset the Zn^{2+} tolerance of the original 293-bp intron sequence.

Discussion

Zn^{2+} has been a subject of studies on metal ion-DNA interactions since the 1960s[11] but much attention has been attracted to its ability to induce B- to Z-DNA transition[15] and convert B-DNA to M-DNA by directly replacing the imino protons of thymine/guanine bases in the double helix[18]. While the influence of this well-known transition metal ion on the structure and physical properties of the DNA double helix is widely recognized, the biological relevance is still uncertain, largely because the related studies were often done under non-physiological conditions, e.g., the observed B- to Z-DNA transition involves the co-existence of certain organic compounds such as ethanol or ethylene glycol[16] while the formation of M-DNA depends on alkaline conditions (pH = 8–9)[18]. Meanwhile, the interaction between Zn^{2+} and ssDNA has been largely untouched and the questions if and how such interaction could affect the annealing of complementary sequences have not been brought to attention in the field.

In the presented study, the Zn^{2+}-ssDNA interaction was first investigated using a simple and sensitive LTEAGE procedure coupled with UV-Vis spectrum and fluorescence quenching analyses. The exclusion of EDTA, which is a strong chelator of divalent ions[19] from the routine agarose gel electrophoresis was the key to success in this study and has not been reported in previous studies. This simple method should be generally applicable for future studies on metal ion-DNA interactions, especially those requiring high-throughput tests that may not be feasible for the application of sophisticated technologies such as X-ray absorption spectroscopy and nuclear magnetic resonance. More meaningfully, the Zn^{2+}-ssDNA interaction was studied in solutions with near neutral pH (7.5) at body temperatures (37°C) that fit physiological conditions. The concentration of NaCl (e.g., 10 mM) tested in this study was much lower than that of physiological saline (~150 mM), however, it is just within the ranges as measured for the nucleus of eukaryotic cells as reported in previous studies[20,21].

Regarding the concentrations of Zn^{2+} in the annealing solutions, it is known that in routine lab stock solutions, free Zn^{2+} could be <0.1% of the calculated molar concentration due to natural oxidation[30,31], thus, the minimal Zn^{2+} concentrations required for blocking DNA annealing as reported in this study (50–100 μm) might be actually at nanomolar levels, i.e., 50–100 nM, which is close to the estimated concentrations of intracellular free Zn^{2+} at least in certain types of living cells as reported by several research groups specializing in zinc biology-related areas[29–32]. The physiological concentrations of intranuclear free Zn^{2+} is largely unknown, but is expected to be significant as observed at least in the mammalian cells under oxidative stress[8,9]. It is not unreasonable to assume that the observed Zn^{2+} blocking events might occur not only in *vitro* but also in the nucleus, which accumulates 30–40% of the total zinc in the human body[1]. Certainly, this possibility would depend on a yet-to-be determined factor that the Zn^{2+}-ssDNA interaction must be strong and quick enough to compete with protein-DNA interactions associated with various DNA synthesis/repair pathways[10,33,34]. Nevertheless, there are reasonable chances for the "naked" ssDNA to be exposed, at least transiently, to intranuclear free Zn^{2+}, e.g., upon the collapse of the DNA replication forks in which the replication proteins become disassembled and fall off the ssDNA templates, leading to the accumulation of ssDNA at the stalled replication forks[33,34].

What would be the biological consequences if the observed Zn^{2+} blocking event *does* occur in a living cell? Single-stranded DNA is an essential intermediate in DNA replication, repair, recombination, and transcription, and must be processed timely[10]. For example, double-stranded DNA breaks (DSBs) occur frequently in eukaryotic genomes due to the attacks of reactive oxygen species (ROS) and in order to repair the DSBs, the 3′-overhangs must be extended and subsequently annealed between complementary partners[28]. Since ROS also causes free Zn^{2+} sparks in the nucleus[8], it is not hard to image that ROS-released Zn^{2+} could block DSB repair if the 3′-overhangs contain Zn^{2+}-sensitive sequences as shown in the end-joining tests mimicking this process (Fig. 4). As suggested by the denature-renaturation tests carried out in this study (Fig. 5), Zn^{2+} could block the annealing of ssDNA as long as 1,635 bp, which could be in the size ranges of ssDNA involved in homologous recombination-dependent DNA repair critical for the reactivation of stalled DNA replication forks caused by DNA damages common in living cells[35,36]. A failure in rescuing the stalled replication forks could lead to catastrophic consequences including cell death and aberrant cell-division[33–36].

The presence of intracellular histochemically reactive free or labile Zn^{2+} (usually detectable at nano- to micromolar levels) is under the control of zinc homeostasis pathways[30–32]. Disturbances on the balance of intracellular free Zn^{2+} have been linked to apoptosis/programmed cell death-related processes in several types of human cells[37,38] and in plant embryos[39]. Excess free intracellular free Zn^{2+} has been associated with brain injuries and neuronal disorders such as Alzheimer's disease[30,38], and in several types of human cancer cells, especially those of the breast and lung cancers in which the free Zn^{2+} levels are significantly higher than in normal cells[40]. A previous study has shown that Zn^{2+} inhibits DNA replication in the human pathogenic bacterium *Salmonella enteric* under phagocytic ROS attack in which the inhibition of DNA replication is always accompanied by intracellular Zn^{2+} mobilization[41]. Although these observations were likely due to the disturbance of Zn^{2+} on the functions of various pathway proteins, the data obtained in this study imply that the Zn^{2+}-ssDNA interaction may be also responsible for cell death and/or tumor growth caused by a dysfunctional DNA replication/repair machinery.

The fact that the Zn^{2+}-tolerant intronic DNA may provide annealing protection on otherwise Zn^{2+}-sensitive coding-DNA (Fig. 5) implies further the biological relevance of the Zn^{2+}-ssDNA interaction. Eukaryotic genomes often contain large amounts of repetitive

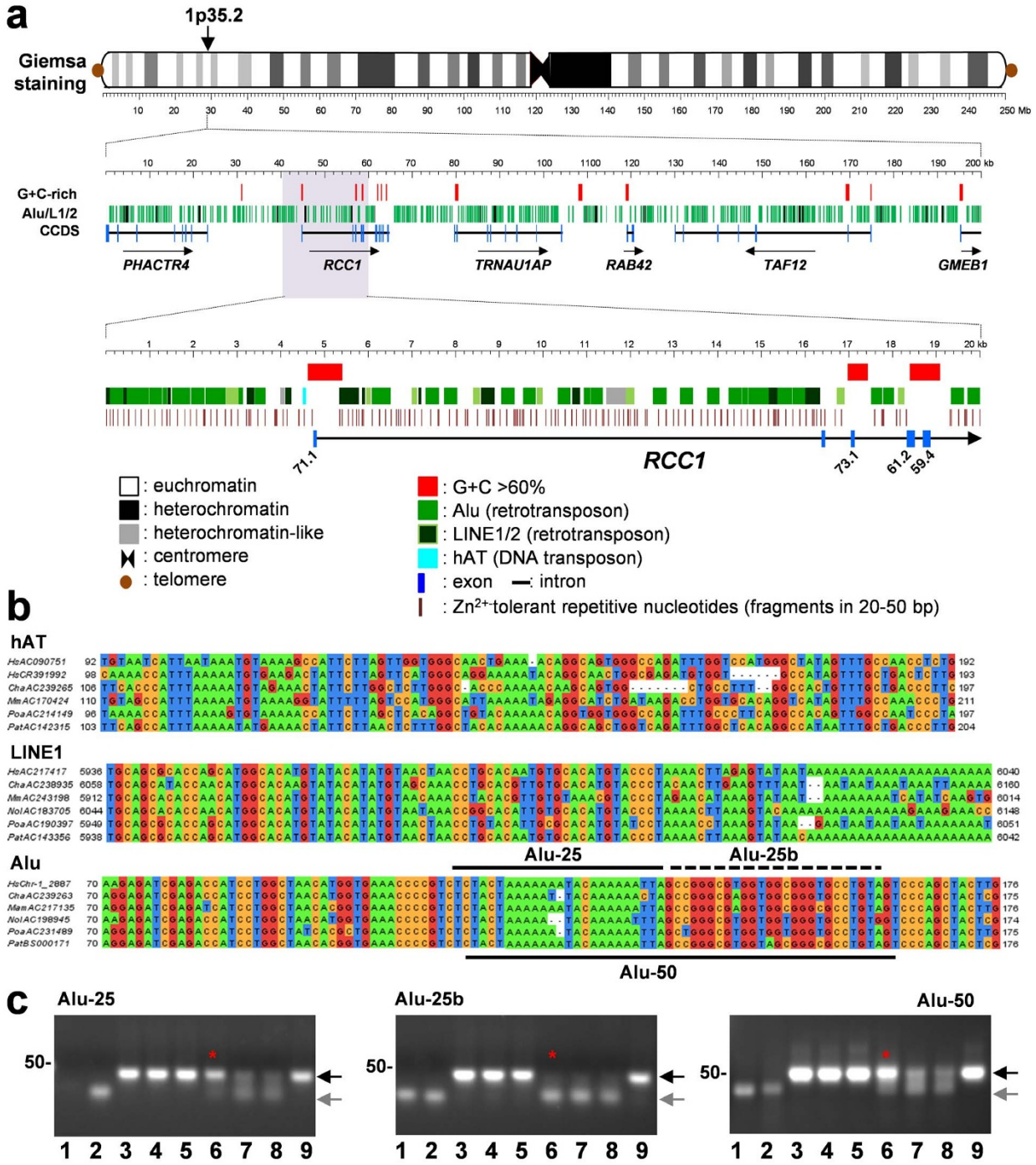

Figure 6 | Zn^{2+}-tolerant repetitive DNA associated with transposable elements (TEs) in human genome. (a) Euchromatin, heterochromatin and euchromatin-associated TEs in human chromosome 1. Idiogram with G-bands (adapted from ncbi.nlm.nih.gov/projects/mapview) is shown at the top, a 200-kb region (positions 28.8-29 Mb of the annotation release 105) with an enlarged segment (20 kb) is shown below. Protein-coding genes are indicated by arrows/letters with numbers below the exons indicating the G+C content (%). *RCC1*: Regulator of chromosome condensation protein 1. (b) Alignments of major TEs in humans and other five primate species. A, T, G and C bases are shown in green, blue, red and orange background, respectively (complete alignments available upon request). Species abbreviations (with GenBank accession numbers): *Homo sapiens*/human (Hs), *Macaca mulatta*/Rhesus monkey (Mm), *Chlorocebus aethiops*/grivet monkey (Cha), *Gorilla gorilla*/gorilla (Gog), *Nomascus leucogenys*/gibbon ape (Nol), *Pan troglodytes*/chimpanzee (Pat), *Pongo abelii*/Sumatran orangutan (Poa). (c) Gel images showing the annealing patterns of DNA oligos representing the Alu sequence in B (thick or dashed lines). Note that Alu-50 which includes both Alu-25 (Zn^{2+}-tolerant) and Alu-25b (Zn^{2+}-sensitive) was Zn^{2+}-tolerant (compare at red asterisks). Lane organization and labelling are the same as those in Figure 1b.

DNA (>50% in humans and up to 80% in plants such as wheat), mainly transposable elements (TEs)[42,43]. The justification for us to live with so much junk DNA[44] has never been resolved univocally[45,46]. Eukaryotic genomes are usually organized as alternative blocks of euchromatin (relatively G+C-rich) and heterochromatin (all A+T-rich), and TEs are found predominantly in the euchromatin regions as shown for the human chromosome 1 (250 Mb) (Fig. 6a), in which all TEs contain short sequences (usually 20–50 bp) similar to those of Zn^{2+}-tolerant repetitive DNA examined in this study, especially, poly(dA)/(dT) stretches (Supplementary Table S4). These repetitive

elements are organized in concert so that the G+C-rich exonons/promoter-related DNA sequences (which, at least for some, have apparent homologues in bacteria) are all separated by TE-embedded intronic or intergenic regions containing Zn^{2+}-tolerant segments almost every 100–200 bp (Fig. 6a). Some of TEs are well conserved in closely-related species (Fig. 6b) and were tested to be Zn^{2+}-tolerant as shown for Alu (Fig. 6c) which takes up >10% human genome[47]. Similar TE-dominant organization was also found in plant chromosomes such as those in wheat (Supplementary Fig. S6).

Do these observations mean we need junk DNA to be able to survive free Zn^{2+} attack while heavily relying on it to make numerous nuclear proteins to keep our genome alive? The human telomeric DNA all end up with a single-stranded tip (100–200 bp) consisting of exclusively the TTAGGG-like simple repeats[24] that are Zn^{2+}-tolerant as shown in this study (Fig. 2c). This may be a direct example to address how smartly a linear chromosome has evolved in the Zn^{2+}-rich nucleus of eukaryotic cells. For the whole genome of any eukaryotic organisms, it sounds quite reasonable that with some junk DNA sticking or jumping around, they may live with Zn^{2+} more safely despite having to pay for the evolutionary by-products, notoriously, the TE insertion-induced genetic diseases in humans[47] or the strange colors on kernels of cereal plants[48]. Although much more need to be done both *in vitro* and *in vivo* before drawing any conclusions, the data obtained in this study have raised a challenging hypothesis that the Zn^{2+}-ssDNA interaction might be among natural forces driving the eukaryotic genomes to maintain junk-like repetitive DNA for adapting to the Zn^{2+}-rich nucleus.

Methods

DNA oligonucleotides. DNA oligonucleotides (24–50 nt) were designed manually and selected carefully against self-complementarity. Selected oligos were synthesized at Sigma Genosys (Sigma Aldrich) with desalting purification and prepared as 10 μm working solutions in nuclease-free water (Ambion-Invitrogen) and stored at −20°C. Sequences of the synthesized DNA oligos are given in Supplementary Table S1.

Annealing assays. Zn^{2+}, Mg^{2+} and Mn^{2+} solutions were prepared from zinc sulfate ($ZnSO_4$), magnesium sulfate ($MgSO_4$) and manganese sulfate ($MnSO_4$), respectively, as 1 M stock solutions in ultrapure water obtained using the Milli-Q-Gradient purification system (Millipore) and stored at room temperature after autoclaving. The stock solutions were diluted to desired concentrations with ultrapure water just before use. For annealing assays, DNA oligo (2 μm) was suspended in 20 μl of solution (10 mM NaCl, 10 mM Tris pH 7.5) containing metal ions at a final concentration 0–750 μm, incubated at 37°C for 10 min. Metal ion-DNA solutions containing complementary ssDNA were then mixed at equal molar concentrations and allowed to anneal at 37°C for 30 min to 12 h. Three types of controls were included in all annealing assays, a DNA solution containing the plus (+) or the minus (−) strand of ssDNA alone without metal ions, and an annealing solution containing a metal ion at 750 μm plus EDTA (1 mM). Annealed DNA samples were separated using the low-temperature EDTA-free agarose gel electrophoresis (LTEAGE) procedure, in which the ethidium bromide-containing gel (1–2.5%) was run at 4°C in Tris-acetate buffer (pH 8.0) without EDTA at 110 V for 25–30 min. Gel images were taken using the Gel Logic 200 System (Kodak).

UV-Vis spectrum analysis. Aliquots (100 μl) of solutions (10 mM NaCl, 10 mM Tris pH 7.5) containing ssDNA (1 μm) and metal ions (0–750 μm) or metal ion (750 μm) plus EDTA (1 mM) (control) were incubated in a 96-well clear microtiter plate (Corning) at 37°C for 10 min before scanning for absorbance at 260 nm (A260) and 295 nm (A295) using a Synergy H1 microplate reader (BioTek) with default settings for pathlength correction. A buffered solution without DNA was included as the blank control in all experiments. The A295/260 ratio (A*), which is an indicator of metal ion-DNA interactions[16], was calculated and used to compare the relative Z^{2+} binding potential (SD^Z) of individual ssDNA using the formula $(A^*_{250}- A^*_0)/A^*_0$ as described in the Results.

Fluorescence quenching assay. The plus strand was dual-labeled in a way adapted from a previous study[49] with Cy3 as the 5′ fluorophore and BQH2 as the 3′ quencher (Sigma). Aliquots (100 μl) of solutions (10 mM NaCl, 50 mM KCl, 10 mM Tris pH 7.5) containing the minus strand (0.2 μm) were pre-incubated with 0–500 μm metal ions in a 96-well black microtiter plate (Corning) at 37°C for 10 min. Probe was then added at an equal molar concentration and incubated at 37°C for 10 min. Fluorescence was detected using the microplate reader mentioned above with fluorescent settings for excitation/emission = 540/570 nm. Relative fluorescence unit (RFU) was calculated by normalizing FU of the annealing solution to the "blank" control which contained the probe only in presence of the metal ions.

DNA renaturation tests. The genomic and coding sequences of the wheat *ACT1* gene (GenBank accession numbers KC775780 and KC775781, respectively) were amplified by PCR/reverse transcriptase PCR as described previously[50] and the PCR products were cloned into a pCR2.1 vector using the TOPO TA Cloning Kit (Invitrogen) and sequenced at Cornell University Biotechnology Resource Center. Double-stranded DNA fragments were amplified by PCR using primers given in Supplementary Table S3 and PCR products were purified using the QIAquick PCR Purification Kit (Qiagen). Purified dsDNA fragments were eluted in nuclease-free water with the final concentration adjusted to 100 ng/μl in 10 mM NaCl, 10 mM Tris pH 7.5 and stored at −20°C. For renaturation assay, dsDNA fragments were denatured by boiling for 10 min then chilled on ice for >10 min. Metal ions were then added to the denatured DNA samples (kept on ice) at a final concentration 0–750 μm and incubated for 10 min before allowing to renature at 37°C overnight.

Statistical analysis. Absorbance and fluorescence measurements were done on at least three replicates for each treatment, and the readings were normalized to the blank control and further processed using the Gen5 2.0 Software (BioTek) (representative data sets including means and standard deviations are given in Supplementary Table S2) and subjected to *t*-test with the significant differences between treatments defined at $P < 0.05$.

Sequence analysis. DNA hairpin structures were predicted using the mfold Web Server (http://mfold.rna.albany.edu)[51] with default parameters for linear oligomers except the ionic condition which was set at 10 mM Na^{2+}, 1 mM Mg^{2+}. Predicted stable folding structures (e.g., ΔG <1) were examined and the representatives were chosen for analysis as shown in related figures. Nucleotide sequences of human chromosome 1 (complete) and wheat chromosome 3B (partial) and the representative transposable elements (TEs) from different species were obtained from GenBank databases. Genes on human chromosome 1 were annotated following on the NCBI annotation release 105 (http://www.ncbi.nlm.nih.gov/projects/mapview). G+C-rich (>60%) islands were identified using the CpG Island Searcher Server (http://www.cpgislands.com)[52] and human TEs were identified by searching the Dfam database (http://www.dfam.org)[53] Sequence analysis and alignment were performed using the Lasergene software (DNASTAR).

1. Vallee, B. L. & Falchuk, K. H. The biochemical basis of zinc physiology. *Physiol. Rev.* **73**, 79–118 (1993).
2. Berg, J. M. & Shi, Y. The galvanization of biology: a growing appreciation for the roles of zinc. *Science* **271**, 1081–1085 (1996).
3. Andreini, C., Banci, L., Bertini, I. & Rosato, A. Counting the zinc-proteins encoded in the human genome. *J. Proteome Res.* **5**, 196–201 (2006).
4. Broadley, M. R. *et al.* Zinc in plants. *New Phytol.* **173**, 677–702 (2007).
5. Cousins, R. J. & Lee-Ambrose, L. M. Nuclear zinc uptake and interactions and metallothionein gene expression are influenced by dietary zinc in rats. *J. Nutr.* **122**, 56–64 (1992).
6. Zhou, B. *et al.* Structural basis for the interaction of a hexameric replicative helicase with the regulatory subunit of human DNA polymerase alpha-primase. *J. Biol. Chem.* **287**, 26854–66 (2012).
7. Lehmann, E., Brueckner, F. & Cramer, P. Molecular basis of RNA-dependent RNA polymerase II activity. *Nature* **450**, 445–449 (2007).
8. Spahl, D. U. *et al.* Regulation of zinc homeostasis by inducible NO synthase-derived NO: nuclear metallothionein translocation and intranuclear Zn^{2+} release. *Proc. Natl Acad. Sci. USA* **100**, 13952–13957 (2003).
9. Tuncay, E. *et al.* Intracellular free zinc during cardiac excitation-contraction cycle: calcium and redox dependencies. *Cardiovasc. Res.* **89**, 634–642 (2011).
10. Watson, J. D. *et al. Molecular Biology of the Gene* (Cold Spring Harbor Laboratory Press, New York, , NY USA, 2013).
11. Eichhorn, G. L. Metal ions as stabilizers or destabilizers of the deoxyriboucleic acid structure. *Nature* **194**, 474–475 (1962).
12. Kang, S. & Wells, R. D. Zinc destabilizes DNA Watson-Crick pairs at AGCT. *J. Biol. Chem.* **269**, 9528–9532 (1994).
13. Laundon, C. H. & Griffith, J. D. Cationic metals promote sequence-directed DNA bending. *Biochemistry* **26**, 3759–3762 (1987).
14. Han, W., Lindsay, S. M., Dlakic, M. & Harrington, R. E. Kinked DNA. *Nature* **386**, 563 (1997).
15. Fazakerley, G. V. Zinc Z-DNA. *Nucleic Acids Res.* **12**, 3643–3648 (1984).
16. van de Sande, J. H., McIntosh, L. P. & Jovin, T. M. Mn^{2+} and other transition metals at low concentration induce the right-to-left helical transformation of poly[d(G-C)]. *EMBO J.*, **1**, 777–782 (1982).
17. Martinez-Balbas, A. & Azorin, F. The effect of zinc on the secondary structure of $d(GA.TC)_n$ DNA sequences of different length: a model for the formation *H-DNA. *Nucleic Acids Res.* **21**, 2557–2562 (1993).
18. Wettig, S. D., Wood, D. O., Aich, P. & Lee, J. S. M-DNA: A novel metal ion complex of DNA studied by fluorescence techniques. *J. Inorg. Biochem.* **99**, 2093–2101 (2005).
19. Chen, Z., Sun, Q., Xi, Y. & Owens, G. Speciation of metal-EDTA complexes by flow injection analysis with electrospray ionization mass spectrometry and ion chromatography with inductively coupled plasma mass spectrometry. *J. Sep. Sci.* **31**, 3796–3802 (2008).

20. Dick, D. A. The distribution of sodium, potassium and chloride in the nucleus and cytoplasm of Bufo bufo oocytes measured by electron microprobe analysis. *J. Physiol.* **284**, 37–53 (1978).
21. Paine, P. L., Pearson, T. W., Tluczek, L. J. & Horowitz, S. B. Nuclear sodium and potassium. *Nature* **291**, 258–259 (1981).
22. Kejnovsky, E. & Kypr, J. Millimolar concentrations of zinc and other metal cations cause sedimentation of DNA. *Nucleic Acids Res.* **26**, 5295–5299 (1998).
23. Isidore, E. *et al.* Ancient haplotypes resulting from extensive molecular rearrangements in the wheat A genome have been maintained in species of three different ploidy levels. *Genome Res.* **15**, 526–536 (2005).
24. Brown, W. R. *et al.* Structure and polymorphism of human telomere-associated DNA. *Cell* **63**, 119–132 (1990).
25. Mergny, J. L., Phan, A. T. & Lacroix, L. Following G-quartet formation by UV-spectroscopy. *FEBS Lett.* **435**, 74–78 (1998).
26. Kabelac, M. & Hobza, P. Na^{+}, Mg^{2+}, and Zn^{2+} binding to all tautomers of adenine, cytosine, and thymine and the eight most stable keto/enol tautomers of guanine: a correlated ab initio quantum chemical study. *J. Phys. Chem. B*, **110**, 14515–14523 (2006).
27. Soler-Lopez, M. *et al.* Interaction of zinc ions with d(CGCAATTGCG) in a 2.9 A resolution X-ray structure. *J. Biol. Inorg. Chem.* **7**, 533–538 (2002).
28. McVey, M. & Lee, S. E. MMEJ repair of double-strand breaks (director's cut): deleted sequences and alternative endings. *Trends Genet.* **24**, 529–538 (2008).
29. Frederickson, C. J., Koh, J. Y. & Bush, A. I. The neurobiology of zinc in health and disease. *Nat. Rev. Neurosci.* **6**, 449–462 (2005).
30. Thambiayya, K., Kaynar, A. M., St Croix, C. M. & Pitt, B. R. Functional role of intracellular labile zinc in pulmonary endothelium. *Pulm. Circ.* **2**, 443–451 (2013).
31. Thompson, R. B. T. *et al.* Practical aspects of fluorescence analysis of free zinc Ion in biological systems: pZn for the biologist. *Fluorescence sensors and biosensors*, Thompson, R. B., (ed.) 351–376 (CRC Press, Boca Raton, FL USA, 2006).
32. Colvin, R. A., Holmes, W. R., Fontaine, C. P. & Maret, W. Cytosolic zinc buffering and muffling: their role in intracellular zinc homeostasis. *Metallomics* **2**, 306–317 (2010).
33. Bielinsky, A. K. Scarce but scary. *Nat. Genet.* **39**, 707–708 (2007).
34. Yang, J., O'Donnell, L., Durocher, D. & Brown, G. W. RMI1 promotes DNA replication fork progression and recovery from replication fork stress. *Mol. Cell Biol.* **32**, 3054–3064 (2012).
35. Cox, M. M. *et al.* The importance of repairing stalled replication forks. *Nature* **404**, 37–41 (2000).
36. Sogo, J. M., Lopes, M. & Foiani, M. Fork reversal and ssDNA accumulation at stalled replication forks owing to checkpoint defects. *Science* **297**, 599–602 (2002).
37. Bozym, R. A. *et al.* Free zinc ions outside a narrow concentration range are toxic to a variety of cells in vitro. *Exp. Biol. Med. (Maywood)* **235**, 741–750 (2010).
38. Shuttleworth, C. W. & Weiss, J. H. Zinc: new clues to diverse roles in brain ischemia. *Trends Pharmacol. Sci.* **32**, 480–486 (2011).
39. Helmersson, A., von Arnold, S. & Bozhkov, P. V. The level of free intracellular zinc mediates programmed cell death/cell survival decisions in plant embryos. *Plant Physiol.* **147**, 1158–1167 (2008).
40. Franklin, R. B. & Costello, L. C. The important role of the apoptotic effects of zinc in the development of cancers. *J. Cell Biochem.* **106**, 750–757 (2009).
41. Schapiro, J. M., Libby, S. J. & Fang, F. C. Inhibition of bacterial DNA replication by zinc mobilization during nitrosative stress. *Proc. Natl Acad. Sci. USA* **100**, 8496–8501 (2003).
42. Choulet, F. *et al.* Megabase level sequencing reveals contrasted organization and evolution patterns of the wheat gene and transposable element spaces. *Plant Cell* **22**, 1686–1701 (2010).
43. Wicker, T. *et al.* A unified classification system for eukaryotic transposable elements. *Nat. Rev. Genet.* **8**, 973–982 (2007).
44. Ohno, S. So much "junk" DNA in our genome. *Brookhaven symposia in Biology* **23**, 366–370 (1972).
45. Bernstein, B. E. *et al.* An integrated encyclopedia of DNA elements in the human genome. *Nature* **489**, 57–74 (2012).
46. Eddy, S. R. The ENCODE project: missteps overshadowing a success. *Curr. Biol.* **23**, R259–261 (2013).
47. Cordaux, R. & Batzer, M. A. The impact of retrotransposons on human genome evolution. *Nat. Rev. Genet.* **10**, 691–703 (2009).
48. Biemont, C. & Vieira, C. Genetics: junk DNA as an evolutionary force. *Nature* **443**, 521–524 (2006).
49. Johansson, M. K., Fidder, H., Dick, D. & Cook, R. M. Intramolecular dimers: a new strategy to fluorescence quenching in dual-labeled oligonucleotide probes. *J. Am. Chem. Soc.* **124**, 6950–6956 (2002).
50. Lu, S., Friesen, T. L. & Faris, J. D. Molecular characterization and genomic mapping of the pathogenesis-related protein 1 (*PR-1*) gene family in hexaploid wheat (*Triticum aestivum L.*). *Mol. Genet. Genomics* **285**, 485–503 (2011).
51. Zuker, M. Mfold web server for nucleic acid folding and hybridization prediction. *Nucleic Acids Res.* **31**, 3406–15 (2003).
52. Takai, D. & Jones, P. A. The CpG island searcher: a new WWW resource. *In Silico Biol.* **3**, 235–240 (2003).
53. Wheeler, T. J. *et al.* Dfam: a database of repetitive DNA based on profile hidden Markov models. *Nucleic Acids Res.* **41**, D70–82 (2013).

Acknowledgments

The author thanks T. Lewandowski for assisting with PCR experiments and Dr. K.D. Kroncke and Dr. R.B. Franklin for kindly reviewing the original manuscript. This study was supported by USDA-ARS CRIS project 5442-21000-037-00D (to S. Lu in part).

Author contributions

S.L. conceived and performed experiments, analyzed data and wrote the manuscript.

Additional information

Accession code: Nucleotide sequences of the wheat actin gene (*ACT1*) have been submitted to the NCBI GenBank databases under accession numbers KC775780 and KC775781.

Mention of trade names or commercial products in this publication is solely for the purpose of providing specific information and does not imply recommendation or endorsement by the U.S. Department of Agriculture. USDA is an equal opportunity provider and employer.

Supplementary information accompanies this paper at http://www.nature.com/scientificreports

Competing financial interests: The authors declare no competing financial interests.

How to cite this article: Lu, S. Zn^{2+} Blocks Annealing of Complementary Single-Stranded DNA in a Sequence-Selective Manner. *Sci. Rep.* **4**, 5464; DOI:10.1038/srep05464 (2014).